JTTEE5 18:23–34
DOI: 10.1007/s11666-008-9214-0
1059-9630/$19.00 © ASM International

A Universal Method for Representation of *In-Flight* Particle Characteristics in Thermal Spray Processes

W. Zhang and S. Sampath

(Submitted April 6, 2008; in revised form June 5, 2008)

The advent of user-friendly in-flight process diagnostic tools has significantly improved our understanding of thermal spray processes. This paper examines the critical attributes of these diagnostic measurements and the applicability of the nondimensional group parameters as a mapping strategy for data visualization. Specifically, first-order process maps (process-particle interactions) have been addressed by converting the temperature (*T*)-velocity (*V*) of particles obtained via diagnostics into nondimensional group parameters [Melting Index (MI)-Reynolds number (Re)]. This approach provides an improved description of the thermal and kinetic energy of particles and allows for cross comparison of diagnostic data within a given process for different materials, comparison of a single material across different thermal spray processes, and detailed assessment of the melting behavior through recourse to analysis of the distributions. An additional group parameter, Oxidation Index (OI), has been applied to relatively track the oxidation extent of metallic particles under different operating conditions.

Keywords diagnostics and control, particle states, melting index, kinetic energy, Reynolds number

1. Introduction

In recent years, the advent of user-friendly process and particle diagnostic tools has percolated the thermal spray industry. These devices have played a pivotal role in enhancing not only our ability to comprehend the complexities in thermal spray processes, but also allows for minimizing variability and enhancing reliability. A variety of diagnostic strategies are available to measure particle parameters in the thermal spray processes. They range from sophisticated to rudimentary based on the measurement method, interpretation, and analysis. Many of these sensors have now been successfully utilized within the harsh confines of the spray booth.

The principle objectives of these diagnostic devices are to measure the spray plume characteristics namely, the particle velocities, temperatures, trajectories, and size distributions. The basis of this interest relies on a widespread appreciation that the in-flight particle velocity, temperature, and size, to a first approximation, determine the nature of the microstructure and properties of sprayed coatings (Ref 1-5). Different strategies are employed to meet these requirements. They include measurement of *individual particle* parameters within the spray stream (e.g., Tecnar DPV 2000 and Inflight™ integrated particle sensor) as well as *ensemble particle* sensors for group measurements of particle velocities and temperatures (e.g., Tecnar Accuraspray, Oseir Spraywatch, Inflight Particle Pyrometer, Stratonics Thermaviz, etc.) (Ref 2, 6-10). Many of these sensors measure particle temperatures through the use of thermal emission emanating from a molten/semi-molten traveling particle, and, use time-of-flight measurements to extract the particle velocities. Generally, the velocity can be measured with reasonable accuracy. However, the estimation of particle temperatures introduces inaccuracies as they rely on knowledge of emissivity of a material (Ref 8). Furthermore, given the dynamic nature of the process, with associated gradients in chemistry and temperature within a given particle, true determination of particle temperatures continues to offer significant challenges. Nevertheless comparative representation due to effect of process parameters provides opportunities for both process design and reliability assessment.

A direct measurement of particle melting status is extremely difficult since pyrometric technique only provides access to the particle surface temperature. This is particularly important for widely used refractory ceramics such as yttria-stabilized zirconia (YSZ), due to its low thermal conductivity resulting in large temperature gradient along the radial direction. For instance, the particle surface may begin to evaporate even before the core melts, which means surface temperature is not adequate to describe the melting status. For metallic materials sprayed under atmospheric conditions, in-flight oxidation of the particle can affect the reported temperature reading, and the applicable emissivity values can potentially be

W. Zhang and **S. Sampath**, Center for Thermal Spray Research, Department of Materials Science and Engineering, State University of New York, Stony Brook, NY 11794-2275. Contact e-mail: sanjay.sampath@stonybrook.edu.

erroneous. Most sensors measure temperature at a given location and does not take into account in-flight time for a traveling particle. Given large differences in melting points, it is difficult to cross correlate across a variety of materials systems.

In recent years, a number of efforts are underway to enhance the utilization of the diagnostic sensors across the spectrum of thermal spray materials and processes. Vaidya et al. (Ref 11, 12) first introduced the concept of *Melting Index* (MI) to describe the molten state of a given particle by normalizing the measured surface temperature with the dwell time and size. In its simplest rendition, this is assessed as:

$$\mathrm{MI} = \frac{T\Delta t_{\mathrm{fly}}}{D} \qquad \text{(Eq 1)}$$

where T is the measured particle surface temperature, K, D is the particle size, m, and ΔT_{fly} is the particle in-flight time, s, which has the following expression:

$$\Delta t_{\mathrm{fly}} = \frac{2L}{V}, \qquad \text{(Eq 2)}$$

where L is the spray distance, m, and V is the particle velocity, m/s

Through this approach and using the output of DPV 2000 (individual particle velocity, temperature, and size), it is possible to cross compare melting status for a given material across different process conditions. It, however, does not allow comparisons amongst a wide array of materials within a given process. In addition, Eq 1 does not reveal whether or when a particle will start to melt, since it does not contain the information of materials' melting points as well as other properties. Zhang et al. (Ref 13) significantly enhanced the scientific description of MI through the thermal resistance and energy balance analysis. They define MI as the ratio of particle residence time in the flame, ΔT_{fly}, to the total melting time (the total time needed to melt the particle), ΔT_{melt}, e.g.,

$$\mathrm{MI} = \frac{\Delta t_{\mathrm{fly}}}{\Delta t_{\mathrm{melt}}} = \frac{24k}{\rho h_{\mathrm{fg}}} \cdot \frac{1}{1 + 4/\mathrm{Bi}} \cdot \frac{(T_{\mathrm{f}} - T_{\mathrm{m}}) \cdot \Delta t_{\mathrm{fly}}}{D^2} \qquad \text{(Eq 3)}$$

where k is the thermal conductivity, W/mK, ρ is the density of the material in liquid state, kg/m^3, h_{fg} is the enthalpy of fusion, J/kg, and T_{f} is the flame temperature near the in-flight particle, K. T_{m} is the melting point of the material, K, D is the particle size, m, and Bi is the Biot number, defined as:

$$\mathrm{Bi} = hr_{\mathrm{p}}/k \qquad \text{(Eq 4)}$$

where h is the heat transfer coefficient, W/m^{2}K.

An advantage of the Zhang's approach is its nondimensionality, which allows for cross-comparison of melting state among a range of materials. This is a very valuable tool in process diagnostics since a range of thermal spray processes are available. From Eq 3, it can be clearly seen that, if the flame temperature is higher than the melting point of the material, the particle begins to melt and a positive MI value will be obtained. Otherwise, the material will not be molten. A MI value of 1 means that the in-flight time equals to the time needed to get the particle fully molten. A MI equals to or higher than 1 therefore corresponds to fully molten particles. It is therefore clear that, from the value of MI one can judge if the particle is partially molten ($0 \le \mathrm{MI} < 1$), fully molten ($\mathrm{MI} \ge 1$) or unmolten ($\mathrm{MI} < 0$). By comparing the MI values of different particles for either different process conditions or multiple materials, one can determine how well the particles have been melted (positive MI values) or how far are the particles from the onset of melting (negative MI values). Certain uncertainties, however, do remain in Eq 3. For instance, the heat transfer coefficient in Eq 3 can only be obtained from numerical modeling (Ref 14). In addition, particle surface temperature, T, has been used to calculate MI considering the integration of thermal energy exchange history between the in-flight particles and their environment, since it is difficult to monitor the real time flame temperature in the vicinity of the flying particles.

Similar to MI, Vaidya et al. (Ref 11) also used particle *Reynolds number* (Re) as another nondimensional method for describing the kinetic state of a particle.

$$\mathrm{Re} = DV\rho/\mu \qquad \text{(Eq 5)}$$

where μ is the dynamic viscosity, kg/ms.

It has been shown both experimentally and theoretically that Re has significant effect on particle impact, spreading and splat formation during thermal spray due to the fact that the parameter considers both the particle in-flight status and the material properties essential to droplet impact and splat flattening (Ref 5, 15-18). Again, this has the advantage that it is nondimensional and nonmaterial specific, which provides a powerful approach to compare among multiple materials and processes. It does, however, require knowledge or estimation of material viscosity in the melting state, which can be obtained from handbooks and open publications. Deposition efficiency (DE) and splat and coating qualities are significantly affected by molten status. It is essential to represent particle status at impact using the material viscosity in the molten state due to the fact that the studied object in this case is the molten particles, i.e., the fluid that is moving with a certain speed.

It should be noted that in Eq 5 we consider the particle Reynolds number and not the fluid Reynolds number used to calculate the drag forced exerted on the in-flight particles, which takes the form as:

$$\mathrm{Re}_{\mathrm{f}} = \frac{\rho_{\mathrm{f}} D_{\mathrm{p}} \left| \tilde{V} + V' - V_{\mathrm{p}} \right|}{\mu_{\mathrm{f}}} \qquad \text{(Eq 6)}$$

where D_{p} is particle diameter, V' is the velocity fluctuation, $\tilde{V}_{\mathrm{f}}$, ρ_{f}, and μ_{f} are the velocity, density, and viscosity of gas phase around the particle, respectively, and V_{p} is the particle velocity. Since the drag force of a particle is caused by the gas surrounding it, the dynamic viscosity of the gas is used in the above equation to calculate the Re. This parameter plays essential role for in-flight particle drag force calculation as well as the transport properties (Ref 19). It is, however, not relevant to the particle status at impact.

In addition to Re, the in-flight particle kinetic energy can be used to capture the velocity component. In the kinetic energy equation

$$\mathrm{KE} = \frac{1}{2} m V^2 \qquad \text{(Eq 7)}$$

m is the mass of particle, which can be calculated from the in-flight particle size estimation from single particle sensors relating to $m = 1/6(\pi\rho D^3)$. This realizes the consideration of process from the stand point of kinetic energy, which is an important component at impact determining the extent of spreading, flattening, and the nature of splat-substrate and splat-splat contact (Ref 20-22). The advantage of using kinetic energy over Re is the square component of the velocity, which is a better descriptor of the energy state. The disadvantage is that it is not nondimensional.

In contrast to ceramics, oxidation is an important attribute of metallic particle in-flight behavior (Ref 23-26). Not withstanding issues with coating properties, in-flight oxidation can affect diagnostic measurement itself due to changes in particle state. Furthermore, oxidation reactions are exothermic and can boost the metallic particle temperature well beyond the thermal spray imparted heating zone. Zhang et al. employed an order-of-magnitude analysis and one-dimensional thermal network model to investigate the heat and mass transport from the plasma flame to the particles. They derived a dimensionless parameter, *Oxidation Index* (OI), to characterize the oxide content of the in-flight particles (Ref 14).

$$\mathrm{OI} \approx \frac{6(Y_{o,f} - Y_{o,c})}{\rho_l} \frac{W_{ox}}{W_o} \frac{\mathrm{Sh}\rho_f D_{o,f}}{d_p} \frac{L}{V_P d_p} \propto \frac{L}{V_P d_p^2} \qquad \text{(Eq 8)}$$

where L is the spray distance, m, $Y_{o,f}$ and $Y_{o,c}$ are the oxygen concentration in the gas phase and in the particle center, respectively, W_o and W_{ox} are the atomic weight of the oxidant and the oxide product, respectively, Sh is the Sherwood number and it is defined as $\mathrm{Sh} = \frac{2h_m r_p}{\rho_f D_{o,f}}$, $D_{o,f}$ is the diffusion coefficient of the oxygen in the plasma flame, ρ_f is the Favre-averaged gas density around the particle and h_m is the mass transfer coefficient between the particle surface and the environment. It should be noted that the mass transfer coefficient and the oxygen concentration surrounding the particles, which are critical in the OI calculation, can only be estimated from numerical simulation, since it is difficult to measure the real time values in experiments. Equation 7 also reveals that the oxide content increases monotonically with the spray distance, and decreases with increasing particle size and velocity. Instead of using the explicit equation provided earlier, values of $L/V_P d_p^2$ can be used to approximate OI (Ref 14, 27). It has been shown that plotting the experimentally measured oxide content against the OI calculated based on L, V_P and d_p provides reasonable agreement. This method, however, can be only used to compare oxidation level of a certain feed material under different torch operating conditions, but nevertheless represent another valuable representation tool as part of the overall process map strategy.

The objective of this paper is to examine and extend the applicability of these group parameters to enable a universal description of particle state in thermal spray. Both averages and distributions in the data have been analyzed and illustrated through the concept of first-order process maps. Considerations have been provided for both plasma spray and HVOF processes for ceramics and metallic alloys. It is envisioned that these maps will provide not only insights into the process-particle conditions but enable a fundamental methodology for description of particle states in thermal spray processes.

2. Materials and Experimental Methods

The concept of process map envisages a common platform to represent and cross compare data, properties, and mechanisms. Even for a single process, for example plasma spraying, there are many hardware configurations available from different manufacturers. In addition, there are different processes such as HVOF, wire arc spray and flame spray that also could beneficially be investigated by the same methodology. Vaidya et al. (Ref 28, 29) successfully carried out experiments covering different equipments and processes for Ni-5Al and YSZ.

The following spraying systems have been used in this investigation.

Air plasma spray 7MB torch (Sulzer Metco, Westbury, NY, USA) with an 8 mm 'G' nozzle was used with the nonswirl gas distribution. A mixture of nitrogen (N_2) and hydrogen (H_2) gas was used for plasma generation. The powder injector with inner diameter of 1.8 mm was externally located at a 90° orientation with respect to the anode axis.

An integrated diagnostic sensor setup was utilized for the particle state measurement and is shown in Fig. 1 (Ref 30). Detailed diagnostic characterization of the spray plume has been carried out using multiple sensors that are set up in a 3D manner at the Center for Thermal Spray Research (CTSR) at SUNY Stony Brook. The sensors used are Spray Position Trajectory sensor 'SPT' (In-flight Ltd., Idaho Falls, ID, USA), In-flight particle pyrometer 'IPP' (In-flight Ltd., Idaho Falls, ID, USA), and 'DPV 2000' (Tecnar Automation Ltd., Quebec, Canada). Detailed description of these sensors are available in the literature (Ref 7, 28, 31). A large number of particle measurements were acquired (>10,000) with the DPV 2000 at the 'flux center,' which was determined using the 'auto centering' algorithm of DPV 2000. Particle in-flight characteristics (position, temperature, velocity, and size) were collected from 'good particles' within a measurement volume of 1.95 × 0.5 × 0.5 mm^3 at the 'flux center' of the spray stream. Spray stream position was measured using SPT sensor and ensemble temperature was measured using IPP. IPP 'looks' at a cylinder (5 mm in diameter and 50 mm in depth) in the spray stream from the top. Due to the large depth of focus (±25 mm), the spray stream was within the measurement volume at all times. To accommodate the different sensors from the

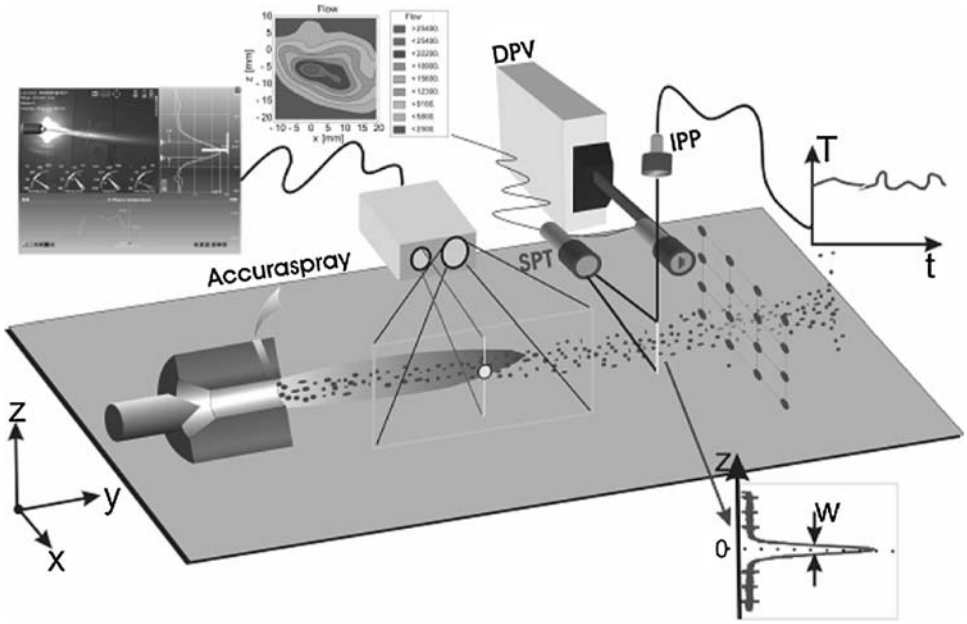

Fig. 1 Integrated diagnostic system used in the experiments (courtesy T. Streibl). All measurements are made at nominal spray distance by moving the torch via robot to measurement location of interest

spray torch, all the sensors cannot be located to view (0 0 0) simultaneously. Instead, the Accuraspray is mounted to view point (0 0 −30), IPP and SPT to view (0 0 0) simultaneously (to realize on-line control of injection, Ref 32) and DPV 2000 to view (0 0 30). By moving the spray torch along the *y*-axis as shown in Fig. 1, the sensor coordinates can be translated to compare data from multiple sensors for the same spray distance. This integrated diagnostic sensor setup provides redundancy, complementary data acquisition, and the opportunity to cross correlate data from different instruments. Data from the SPT and IPP ensemble sensors are not presented in this work. However, it is essential to mention that the quick feedback from these sensors helps to assess data fidelity (Ref 32).

Our previous studies have revealed that the plume position of the particles at injection is critical in determining the heat and momentum transfer for external injection DC plasma spray processes. As one scans through the radial plume position at the point of injection (through stepwise changes in carrier gas flow rate), there is a maxima observed in temperature and velocity of the particles at a fixed plume position for a given torch/nozzle combination. The existence of this ''sweet spot'' is discussed in detail elsewhere (Ref 32). With such an injection strategy, one can achieve the optimum particle state for a given material under a set of parametric conditions. It is pointed out that such an injection optimization step was carried out for most of the materials/process conditions described in this paper particularly those comparing different materials. An added benefit of this strategy is better data fidelity from diagnostics as the particle position in the plume is more appropriately captured.

3. Results and Discussion

3.1 Development of First-Order Process Maps Across a Spectrum of Materials for a Single Process

Process maps are science-based representations of interrelationships among control parameters and measured responses. Such maps provide integrated set of relationships that link processing to properties and ultimately to performance. The map can consist of both experimental and computational data and illustrated to identify key response attributes. Process maps are useful not only because they allow visualization of the process variables, but also enable intelligent control of the process. For example, in a production environment, a well-developed process map can enhance stability and reliability. Process maps also allow one to validate theoretical models and enable model-guided design of experiments. The knowledge obtained in the development of process maps can be both fundamental and practical in nature.

Several past studies have defined and synthesized process maps for thermal spray. Given the multidimensional nature of the thermal spray process, process maps are developed based on torch parameter-particle state relations (referred to as a first-order map) and particle state—coating property responses (referred to as a second-order process map). Details on the synthesis and application of these maps are provided in references (Ref 20, 28). These earlier focused studies have been limited to a single material and/or process and provide a framework for coating design, process parameterization, and property assessment for such a system. The focus of the present investigation is to explore first-order maps

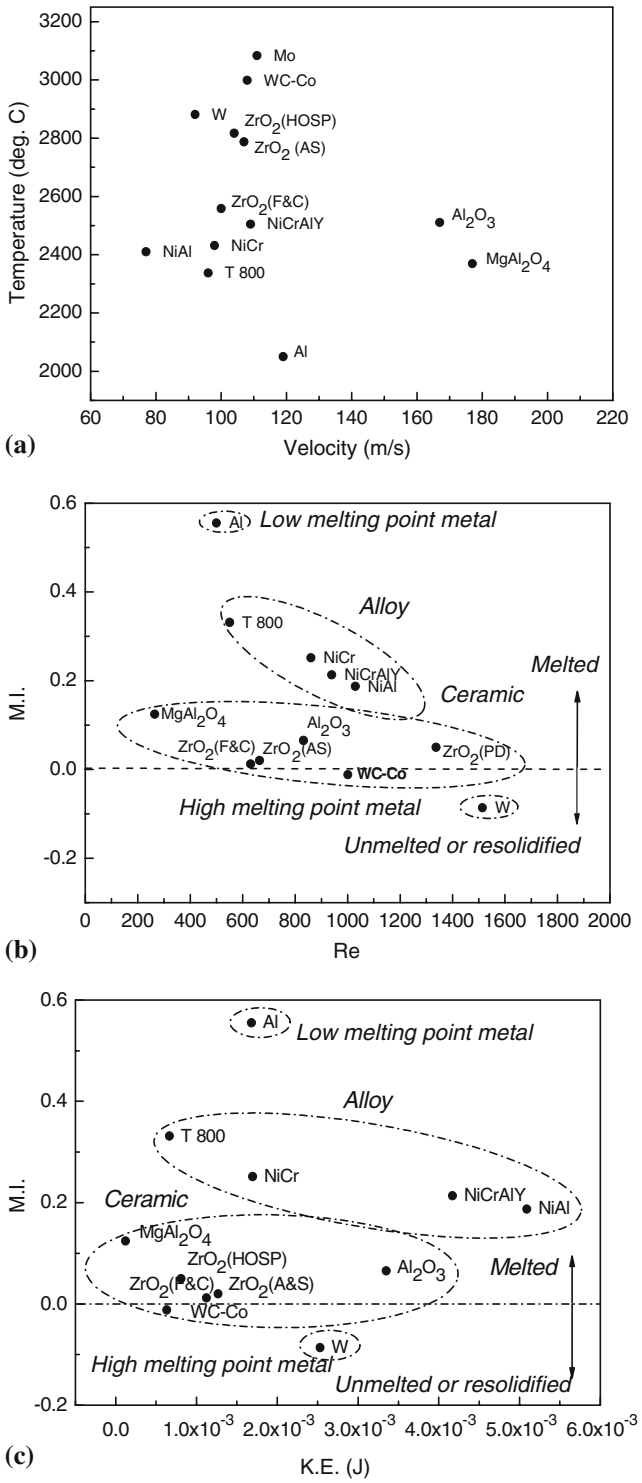

Fig. 2 (a) *T-V* global process map, (b) MI-Re global process map, and (c) MI-KE global process map

with multiple materials and processes. Figure 2 presents a generalized first-order map based on large number of process diagnostic results obtained from multiple materials, and processed through a typical air plasma spray torch at one or more process conditions (as mentioned earlier injection was optimized for each material so as to have maximum heat and momentum transfer for that particular condition). A variety of materials with widely different physical properties have been investigated including metals, ceramics, and cermets. Figure 2(a) is a traditional first-order temperature-velocity representation based on the DPV generated single particle data. At first glance, it is clear that simply using T and V data does not provide an adequate representation of the material behavior within the plasma spray especially to capture the effective energy/temperature gradient within a particle. Aluminum falls on the bottom of the plot while molybdenum and tungsten are on top due to their higher surface temperatures. Furthermore it is inappropriate to compare particle molten status (thermal energy) based only on the surface temperature. For metal particles, the temperature is generally expected to be uniform throughout the particle due to its high thermal conductivity. Thus, the particle surface temperature can be used (to a first approximation) to identify the phase status of the particle (noted that oxidation is an important issue which is considered later in this study). For a ceramic particle, especially those with low thermal conductivity, the particle temperature can potentially differ from a high value at its surface to the center core. A high particle surface temperature above the melting point therefore does not guarantee the particle is fully melted. The melting percentage of the particle depends on its size, thermal conductivity, latent heat, and residence time in the plasma flame. Furthermore, particle velocity cannot provide sufficient information for particle kinetic status at impact considering different physical properties of materials and particle size at impact.

As discussed earlier, group parameters, MI and Re, provide a novel strategy for a more comprehensive description of particle states. The DPV generated single particle data was used to calculate the individual particle's MI and Re numbers, and average values based on these measurements for each of the materials. This is represented in Fig. 2(b) from the T, V, and diameter data obtained for materials in Fig. 2(a). Several important observations can be made.

In the MI-RE based first-order process map, it is clearly seen that low melting point Al shows the highest melting state (value of MI) while W shows the lowest value of MI despite representing a much higher temperature in the *T-V* based first-order process map.

Since MI is a nondimensional group parameter, it is now possible to demarcate a singular melting point (at MI = 0) for all the materials in a single map, i.e. the boundary between molten and un-molten or re-solidified materials. As such the first-order process map can now be used to represent materials that are nominally molten and superheated versus those that are at the cusp of melting.

Most metallic alloys have better molten status compared to oxide ceramics, due to their higher thermal conductivity and lower melting points. By considering these two nondimensional group parameters, MI and Re, the global MI-Re process map successfully represents molten and kinetic status for multiple materials in a single map and as such provides a universal representation

methodology for first-order process maps based on DPV 2000 single particle data.

Similar to the development of MI-Re process map, MI-KE process map can be developed based on the single particle data as shown in Fig. 2(c). The cubic component of particle size and square component of particle velocity in KE equation provide a better way to describe the particle energy state. For example, the KE value for the HOSP ZrO_2 shown in Fig. 2(c) is much smaller than those of F&C and A&S particles, which is opposite to the trend of kinetic status shown in Fig. 2(a) and (b). Considering the fact that the density of the HOSP particles is much smaller than those dense ones, different trends for kinetic status shown by velocity, Re and KE are expected. Thus, this MI-KE process map realizes the consideration of process from the stand point of actual kinetic energy. It also carries most information revealed by a MI-Re map. The disadvantages of the MI-KE maps are, first, it is not nondimensional, and second, the material viscosity which is important for determining the extent of spreading, flattening and splat-splat contact is not included in the KE description.

3.2 Expanded Process Maps: Comparison Across Processes and Materials

A large group of process and materials have been examined by Sampath and Vaidya et al. (Ref 20, 21, 28). Figure 3(a) shows an overview of the 'atlas' presenting the process window for multiple processes and materials in a *T-V* map. This kind of an 'atlas' would be useful to understand process limitations. Within each process, considerable details can be nested in terms of the effects of various control factors that go into the process. Such a map can provide a method to compare operational zones, limits and variabilities for these spraying systems. For identical materials which can be used in different systems, this process map can provide the range of particle characteristics over which it can vary.

Figure 3(b) provides the process window for multiple processes and materials in a MI-Re space. This provides a more fundamental approach to represent particle status using dimensionless scales, which realizes the comparison among multiple materials. The most significant difference in conditions is depicted for the Ni-5Al material for which the data are spread over a very large range in MI-Re space for different spraying systems. This difference is not clear in the *T-V* space due to the fact that the particle size difference in the TWA and APS processes is not visible. As shown in Fig. 3(b), the lower MI and larger Re for the TWA process result from larger particles. The MI-Re process map therefore provides an improved basis for understanding the in-flight particle status.

3.3 Implications of Group Parameters on Materials and Process Assessment: Particle Size Effect in YSZ

Benefits of selecting group parameters are evident for single material with different process or feedstock combinations. Figure 4 shows a first-order process map for

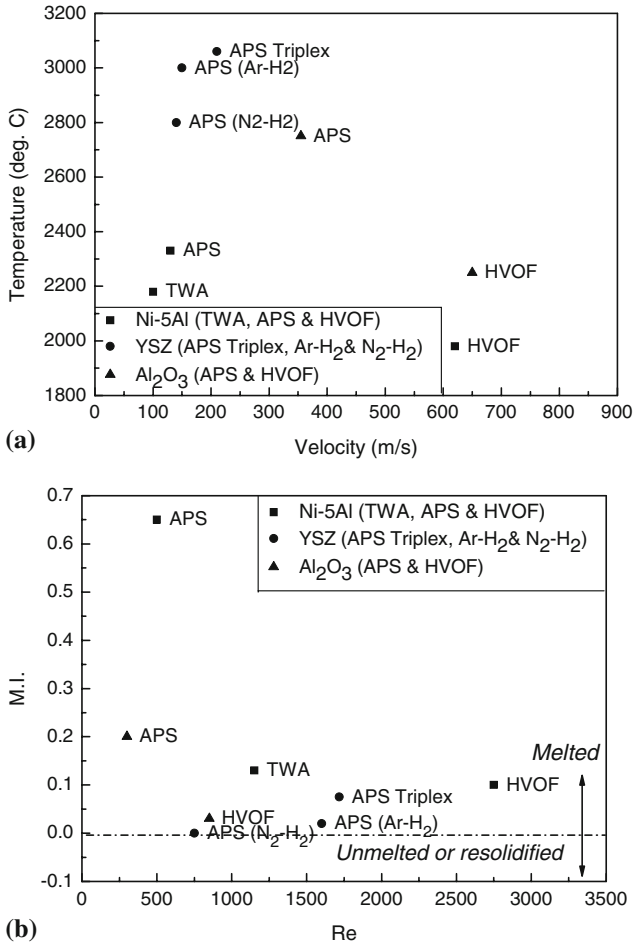

Fig. 3 Global process map for multiple process and materials (a) *T-V* map and (b) MI-Re map

plasma spraying of two types of YSZ powders using two types of nozzles. Both powders were of the plasma densified variety comprising to two size distributions: a fine and a coarse size cuts. Each of the powders was subjected to a variety of plasma spray process conditions using a 6-mm and an 8-mm nozzle diameter. As expected, Fig. 4(a) shows that the 8-mm nozzle produces slower and hotter particles compared to faster and cooler particles. The ellipses represent envelope of *T-V* response for a given feedstock-nozzle combination for a variety of spray parameters (gun current, hydrogen, and primary flow rate). A first-order *T-V* map at first glance suggests that the coarser powder is at higher particle temperatures. This can be attributed to the fact that the reported DPV measurements are primarily from a particle surface and fail to represent the volume thermal energy of the particle.

Replotting the same first-order data through a MI-Re map in Fig. 4(b) clarifies these issues and yields expected results. The MI for coarser powder is somewhat lower than the finer powder while the Re is higher for the coarser powder due to the larger particle diameter. Figure 4 demonstrates the utility of group parameters in

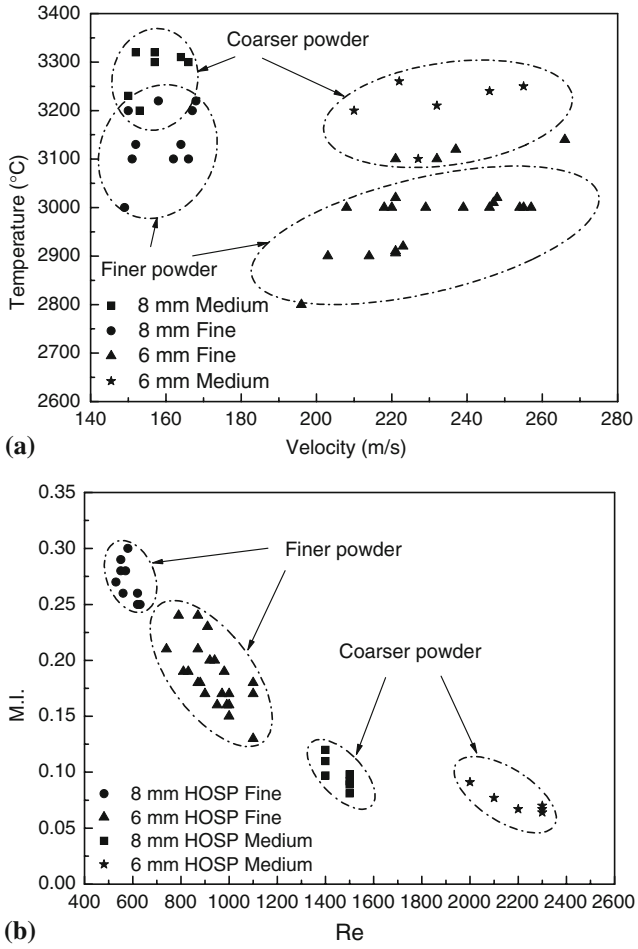

Fig. 4 Nozzle and particle size effect on process window for YSZ (a) *T-V* map and (b) MI-Re map

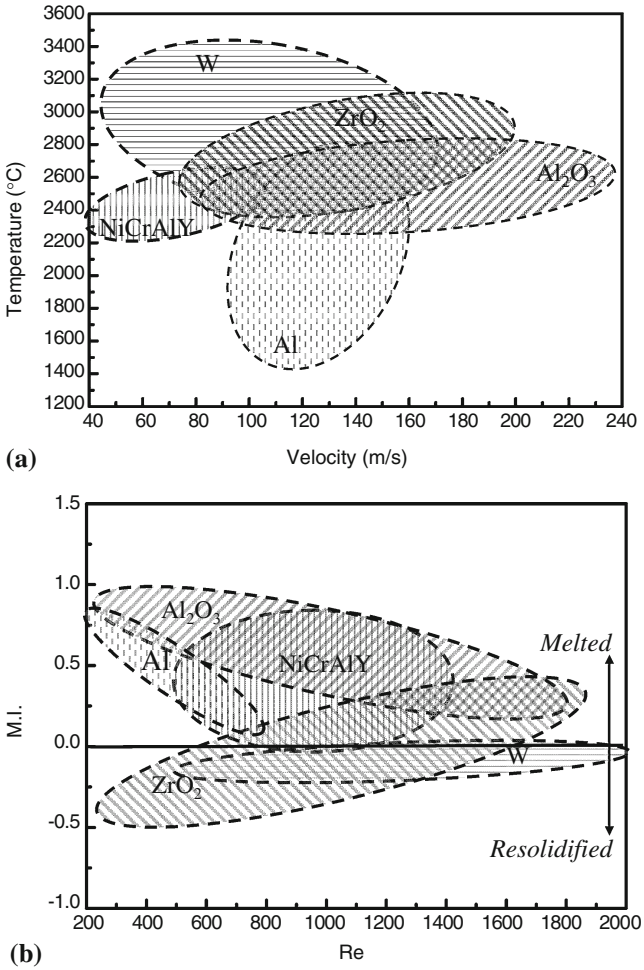

Fig. 5 (a) global process map considering temperature and velocity distribution; (b) global process map considering MI and Re distribution

accurately capturing the process-material responses in the first-order maps.

3.4 Discussion on Distribution

We have thus far reported first-order process maps based on average values of DPV measured single particle data. For the case of MI, calculations were made at the single particle level and then averaged. Average values of the particle conditions, however, are insufficient to completely describe the process. Our earlier work has shown that considerations of temperature distributions are important as they enable identification of the melting state of the materials particularly for refractory oxides (Ref 6).

Another straightforward way to visualize the particle state is to display the entire DPV measured distribution in the first-order map. Figure 5(a) examines such a *T-V* space for several of the materials identified in Fig. 2 encompassing entire DPV output of several thousand spray particles. Each ellipse represents the distribution for each group of particles (same material) in the *T-V* space (the data are truncated to eliminate the outliers which represents $<5\%$ of the total data set). Again simply comparing the temperature-velocity distributions does not adequately capture the observed effects. Figure 5(b) is the corresponding comparison of the MI-RE first-order maps. Superimposing the isomelting line representing the zero value of MI, one can easily discern the effective molten status for the whole group of particles. This is uniquely made possible through our nondimensional mapping strategy. Figure 5(b) captures the material response as well as the melting state and as such provides a more significant method of process visualization.

Melting Index represents the molten status of each single particle and allows for comparison of molten status among multiple materials subjected to similar plasma spray conditions. A quantitative extension to Fig. 5(b) is to calculate the number density of the particles above and below the melting threshold represented by the MI = 0 isotherm for a given material/process condition. This enables calculation of the number density of molten particles. The results presented in Fig. 6 indicate that 32% of the YSZ particles are molten from this specific measured parametric set. Also, based on the value of MI of the

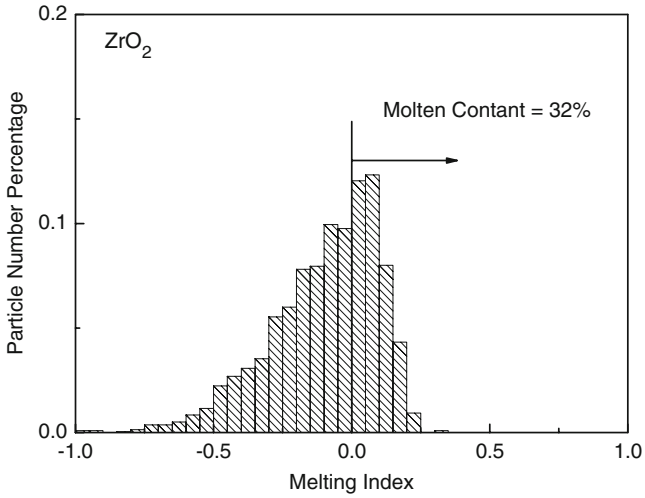

Fig. 6 Molten content: number percentage of molten particles

single particles, one can further compare molten status directly among various materials and processes. As shown in Fig. 7, the updated global process maps (from Fig. 2) consider distributions in MI as per the above paragraph. Comparisons of molten status through different groups of particles for multiple materials are realized. For example, when comparing the MI distribution of ceramics with those of Al and NiCrAlY, it is revealed that most particles from the group of metals and alloys melt much more easily than the two ceramics, even though the whole group of the Al_2O_3 particles has started melting. This allows for a more elaborate comparison of molten status among multiple materials, which cannot be obtained from the information of particle temperature alone. It is also shown in Fig. 7 that, even though NiCrAlY has much higher average MI value (0.33) than that of Al_2O_3 (0.046), the molten content for NiCrAlY (98%) is smaller than that for Al_2O_3 (100%), which means the whole group of Al_2O_3 and 98% of NiCrAlY have been melted to some extent. Another more

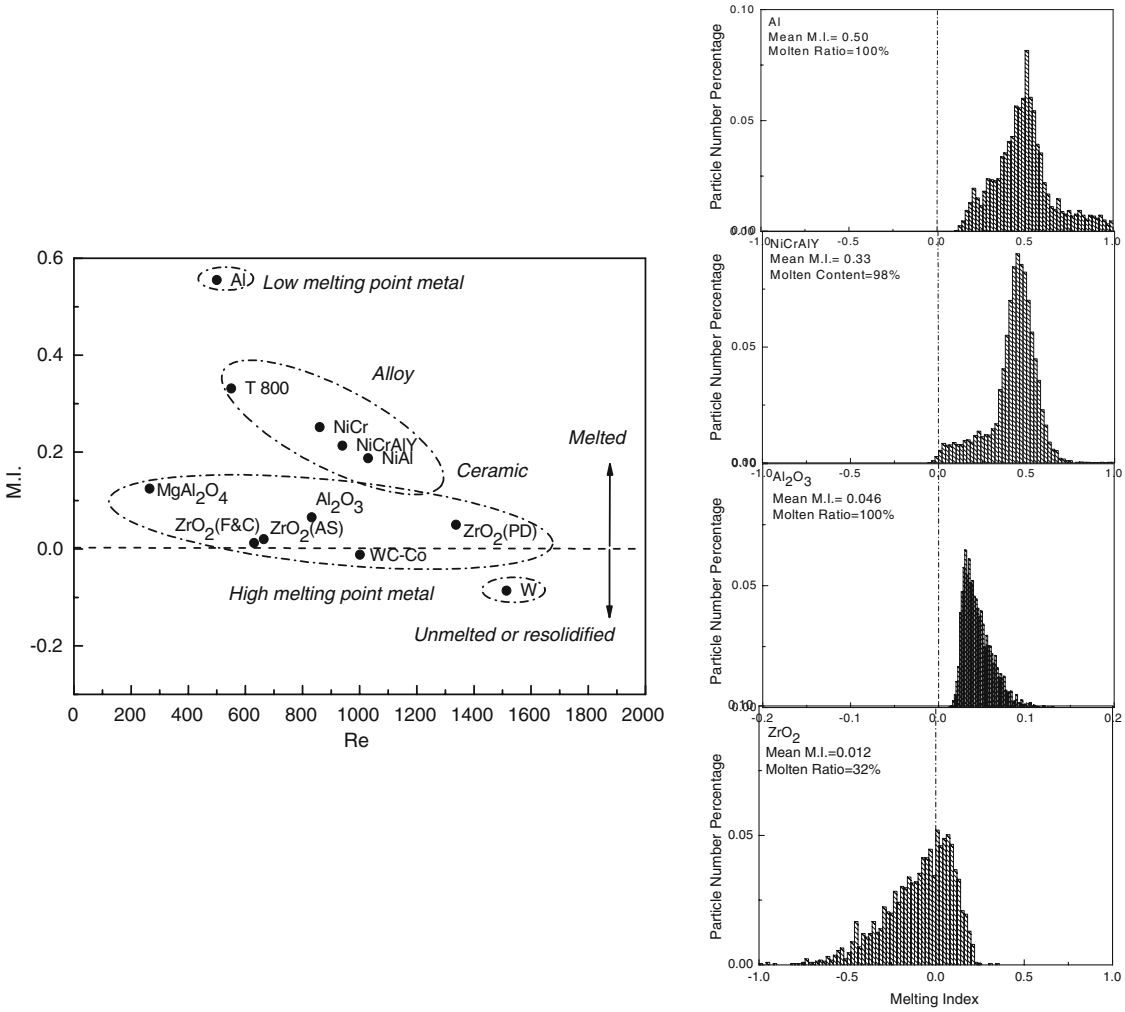

Fig. 7 Statistical representation of global process map

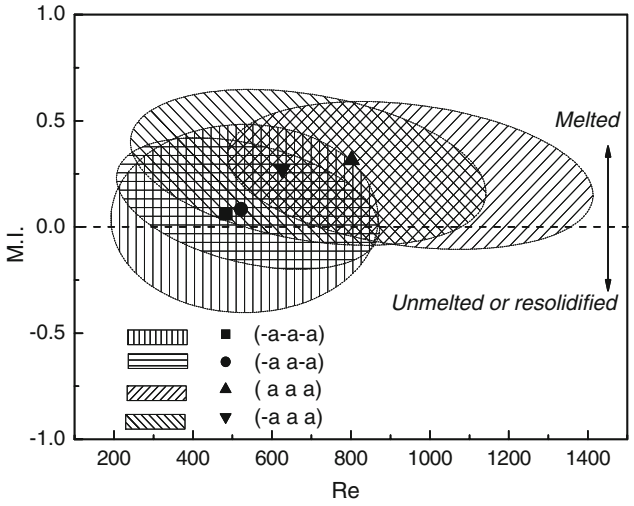

Pattern	Thickness per pass μm	Relative D.E. %	Thermal conductivity W/mK
(a a a)	0.92	100	1.29±0.01
(-a a a)	1.20	86.2	1.13±0.01
(-a a-a)	1.40	26.8	1.0±0.01
(-a-a-a)	1.73	19.8	0.97±0.01

Fig. 8 YSZ process map considering MI and Re distribution

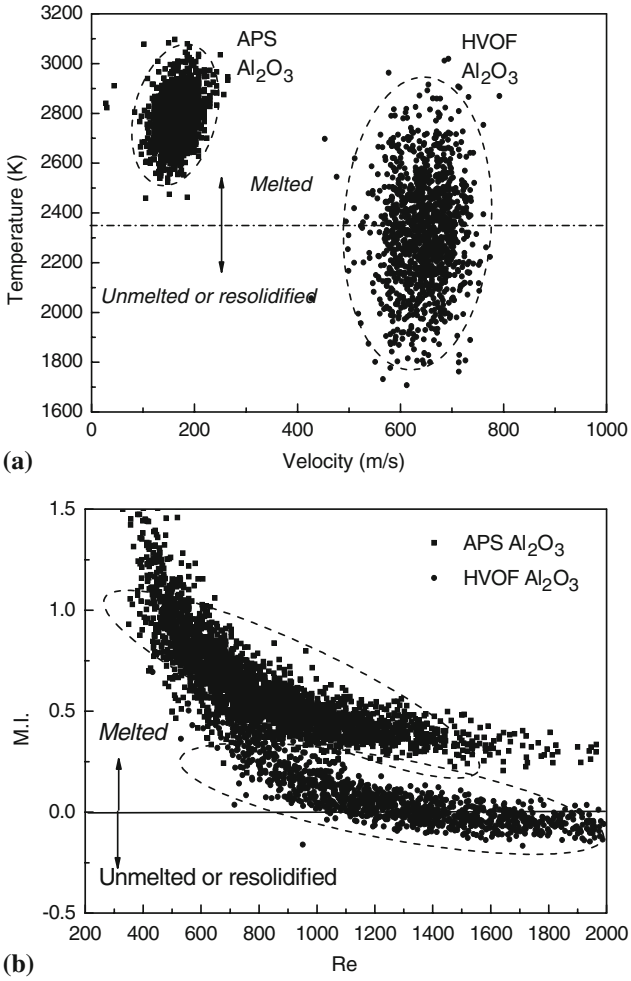

Fig. 9 Al_2O_3 process map considering different processes and (a) temperature, velocity distribution and (b) MI, Re distribution

statistically significant example can be obtained when comparing the distribution of YSZ and that of Al_2O_3. For YSZ, the mean MI is 0.012, which is similar to that of Al_2O_3. However, it is clearly shown that only 32% of the YSZ particles have been melted as shown by the statistical distribution for MI. Checking the distribution provides detailed information for the molten status for a whole group of particles, which cannot be obtained from average of MI for the whole group of particles.

Figure 8 shows the MI-Re distribution maps for YSZ subjected to a variety of processing conditions. The ellipses represent the MI and Re distribution for the whole group of particles under each extreme condition. The average values are also noted within the distribution ellipses. The important parameters relating to coating quality, such as 'thickness per pass' and relative DE, are listed in this figure. It is clearly shown that, with increasing MI and Re, the 'thickness per pass' keeps decreasing, while the relative DE keeps increasing. Increased thermal and kinetic energy causes the flattening and spreading of droplets which favors the formation of dense coatings corresponding to low splat thickness as well as increasing thermal conductivity values as shown in Fig. 8.

First-order process maps can also be used to compare across processes. Figure 9 compares plasma and HVOF process maps for alumina. Since only a single material is compared, the isomelting line can be identified in this *T-V* map. It is clear that the APS Al_2O_3 has much higher molten status than its HVOF counterpart, while the HVOF particles have much higher kinetic energy. The MI-RE map also shows a similar trend although the differences in Re is not as substantial. This relates to the significantly smaller particle size distribution of the HVOF powder feedstock.

3.5 Discussion on Particle Oxidation Status

An important consideration during thermal spraying of metallic particles is in-flight oxidation. In-flight oxidation can introduce both physical changes to the metallic particles (such as extended heating due to exothermic reaction) and chemical changes in terms of the material. The former change needs to be considered in our interpretation of the process-particle state data and will be manifested in some form in the first-order process map, while the latter one can affect the emissivity of the particle and can introduce uncertainties in temperature measurements.

3.5.1 Implication of Oxidation on Particle Temperature. To understand the contribution of the exothermic oxidation on particle temperature, a comprehensive

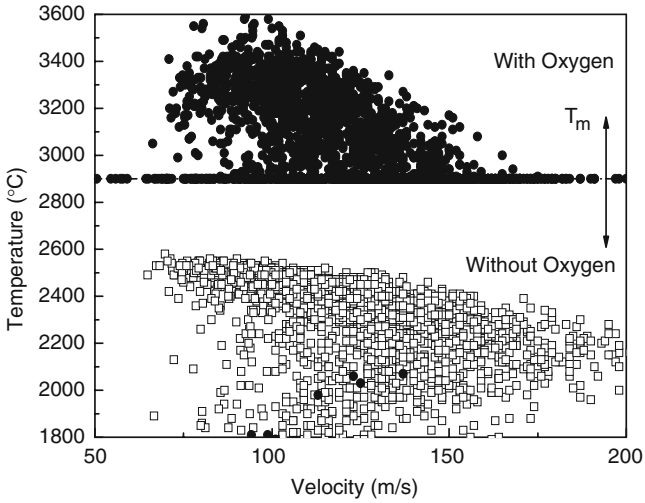

Fig. 10 Oxygen effect on particle in-flight status from simulation

process model, LAVA-3D P, was utilized. The species transport due to convection and diffusion in the gas phase have been considered by LAVA, while species transport due to convection in the molten part of particle has been ignored due to the small size of the particles. Description of the model is beyond the scope of this paper and the readers are referred to extensive peer reviewed literature on the subject (Ref 14, 24). Suffice to note that this model allows us to track individual particles during traditional DC plasma spraying in-flight and enables incorporation of physical mechanisms into the model. Figure 10 compares the particle temperature data for Mo particles with and without oxidation contribution. It is clear that under typical thermal spray conditions the particles undergo substantial increase in temperature due to exothermic oxidation.

3.5.2 Discussion on Oxidation Index. As it is the goal of this paper to develop mapping strategies for particle diagnostic results, we here in explore additional methods of data representation for metals and metal laden composite particles during atmospheric thermal spraying. As discussed earlier, OI is a mean to capture these effects and trends. With the help of single particle sensor, the relative oxide content can be calculated and compared through the same materials. Figure 11(a) and (b) shows the OI-MI and OI-Re process maps for molybdenum particles, respectively. As shown in Fig. 11(a), for the same particle size distribution, larger-sized nozzle will generate slower plasma jet providing enough dwell time for the in-flight particles to be heated up and to have more chance to react with oxygen in the environment, which corresponds to high OI and MI values. On the other hand, the generation of enthalpy for the oxide provides considerable amount of thermal energy to enhance the particle melting. For the same nozzle size, smaller-sized particles has less total heat capacity and high specific area, which favors the heat and mass transfer between the particles and their environment, and results higher values of MI and OI.

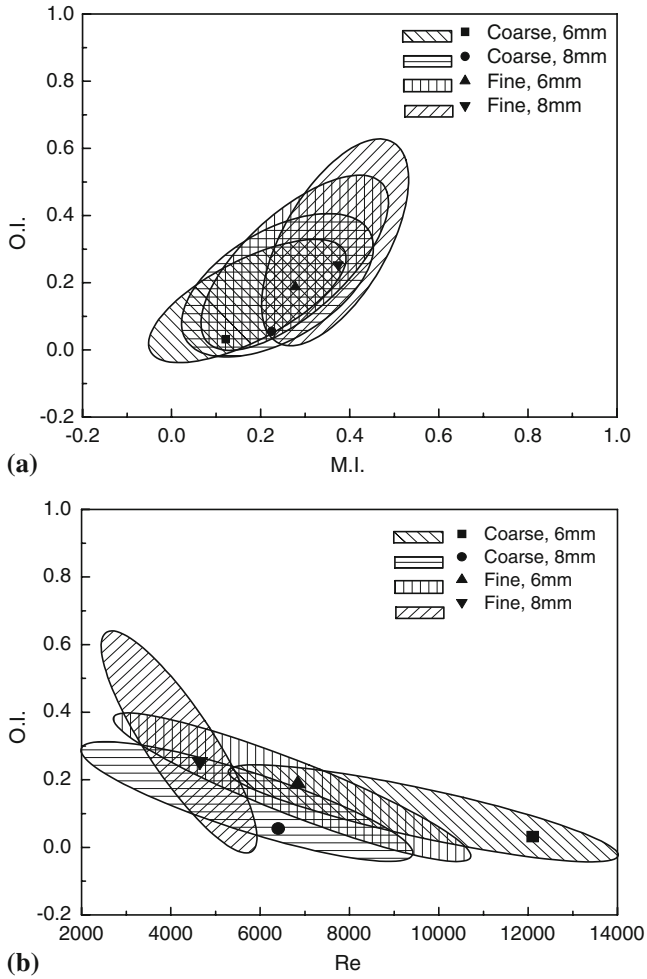

Fig. 11 (a) OI-MI and (b) OI-Re map for molybdenum particles under different combination of nozzle and particle sizes combinations

Figure 11(b) reveals the correlation between the oxidation status and the kinetic energy. For the same initial particle size distribution, decreasing nozzle size dramatically increases the plasma jet velocity as well as the in-flight particle velocity. This reduces the particle dwell time and thus the oxidation content. For the same nozzle size, smaller-sized particles have much larger specific area for oxidation reaction, which result higher oxidation content.

3.6 First-Order Maps Based on Ensemble Particle Diagnostics

The calculation of nondimensional MI-Re maps are enabled in large part due to the availability of single particle type diagnostic sensors such as DPV 2000. In many industrial settings, single particle diagnostics are either not available or not used due to the instrument complexity. Ensemble sensors such an Accuraspray, IPP or SprayWatch are more widely used. This limits our ability to calculate group parameters. Under these circumstances, a simple modification to the *T-V* diagram is to

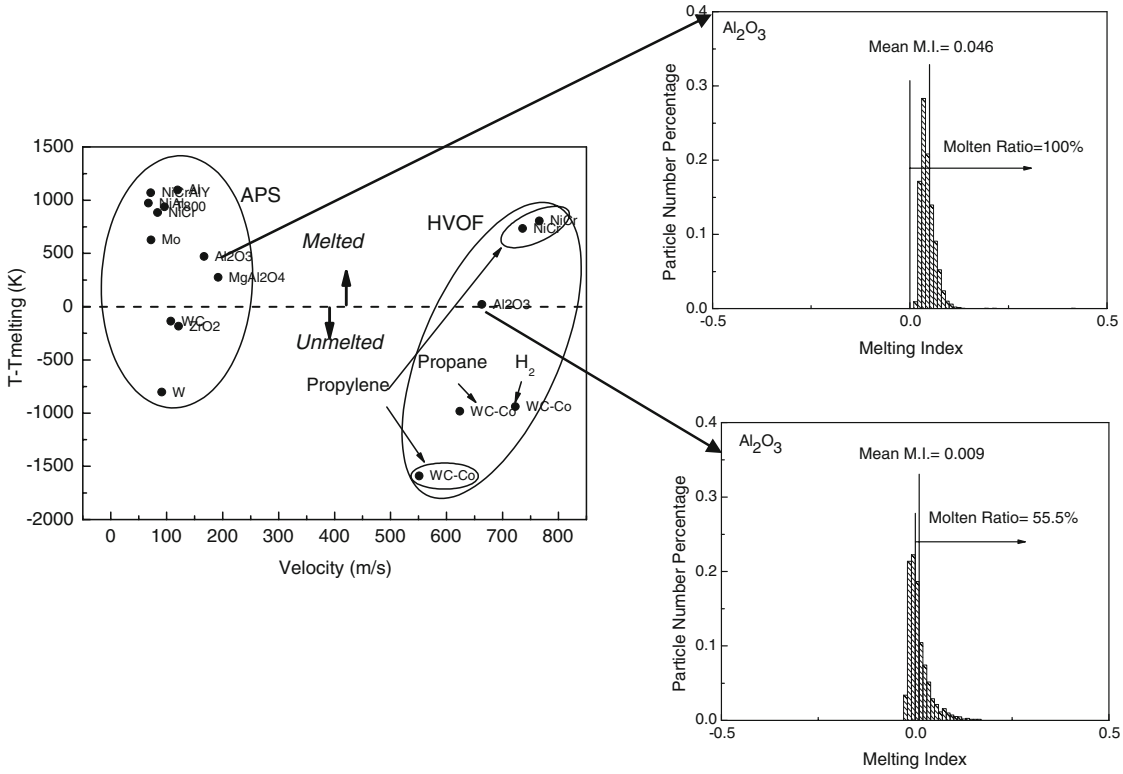

Fig. 12 Global process map considering different processes

represent the temperature data qualified to the melting point (i.e. $T - T_m$). Figure 12 displays these results for a number of APS and HVOF sprayed metals, ceramics, and cermets. The difference between particle surface temperature and the melting point for that corresponding material has been used to represent the particle molten status. The super-imposed dashed line represents the position at which particle surface temperature equals to its melting point. Figure 12 also compares statistical distribution for Al_2O_3 molten status from different spraying systems. Comparing with HVOF process, APS Al_2O_3 particles obtain much higher thermal energy and thus molten status with 100% molten ratio. Again this figure quantifies the fact that the APS process provides higher thermal energy compared with the HVOF process, while lower kinetic energy than its counter part.

4. Conclusions

This paper describes a new strategy for visualization and representation of particle diagnostic results for thermal spray processes. The definition and physical interpretation of nondimensional group parameters, MI and Re, are described and the advantages of using these parameters to represent particle in-flight status are discussed. Another group parameter, OI, has been defined and used to represent a measurement of in-flight oxidation of metallic particles for various parametric conditions. The outcome of such a strategy is a universal method for representation of in-flight particle characteristics in thermal spray processes. This results in a global first-order process map, comparing across a spectrum of materials for air plasma spray process. This new approach offers significant advantages over traditional *T-V* based first-order maps. These maps also allow for representation of molten and kinetic status of multiple materials and can be successfully represented in a unified map.

By expanding the maps to include entire distributions of the MI-Re space, a more comprehensive comparison of molten status among multiple materials can be realized enabling critical cross-comparison of process-material interactions amongst different spraying systems and different materials. OI-MI and OI-Re process maps are used to further reveal particle in-flight status for a certain material under various process conditions. Finally, approximations to the new mapping strategies are proposed in circumstances where only ensemble particle diagnostics are available.

Acknowledgments

This research was supported by the GOALI-FRG of the National Science Foundation under award CMMI 0605704 (co-funded by the division of materials research). The authors are grateful for support received from industry through the Industrial Consortium for Thermal Spray Technology. The authors would also like to

acknowledge of the contributions of Dr. A. Vaidya, Dr. V. Srinivasan, Dr. B.G. Ravi, and Antonio Caccavale in the collection of particle diagnostic data.

References

1. P. Fauchais, Understanding Plasma Spraying, *J. Phys. D Appl. Phys.*, 2004, **37**(9), p R86-R108
2. J.R. Fincke, W.D. Swank, R.L. Bewley, D.C. Haggard, M. Gevelber, and D. Wroblewski, Diagnostics and Control in the Thermal Spray Process, *Surf. Coat. Technol.*, 2001, **146**, p 537-543
3. C. Moreau, J.F. Bisson, R.S. Lima, and B.R. Marple, Diagnostics for Advanced Materials Processing by Plasma Spraying, *Pure Appl. Chem.*, 2005, **77**(2), p 443-462
4. M. Prystay, P. Gougeon, and C. Moreau, Structure of Plasma-Sprayed Zirconia Coatings Tailored by Controlling the Temperature and Velocity of the Sprayed Particles, *J Therm. Spray Technol.*, 2001, **10**(1), p 67-75
5. H.R. Salimijazi, L. Pershin, T.W. Coyle, J. Mostaghimi, S. Chandra, Y.C. Lau, L. Rosenzweig, and E. Moran, Effect of Droplet Characteristics and Substrate Surface Topography on the Final Morphology of Plasma-Sprayed Zirconia Single Splats, *J. Therm. Spray Technol.*, 2007, **16**(2), p 291-299
6. T. Streibl, A. Vaidya, M. Friis, V. Srinivasan, and S. Sampath, A Critical Assessment of Particle Temperature Distributions During Plasma Spraying: Experimental Results for YSZ, *Plasma Chem. Plasma Process.*, 2006, **26**(1), p 73-102
7. K. Landes, Diagnostics in Plasma Spraying Techniques, *Surf. Coat. Technol.*, 2006, **201**(5), p 1948-1954
8. J.R. Fincke, D.C. Haggard, and W.D. Swank, Particle Temperature Measurement in the Thermal Spray Process, *J. Therm. Spray Technol.*, 2001, **10**(2), p 255-266
9. J.A. Brogan, C.C. Berndt, W.C. Smith, R.V. Gansert, S. Raghu, S. Sampath, and H. Herman, Real-Time Imaging of the Plasma Spray Process—Work in Progress, *J. Therm. Spray Technol.*, 1995, **4**(4), p 374-376
10. A.F. Kanta, G. Montavon, M.P. Planche, and C. Coddet, Plasma Spray Process on-Line Control by Artificial Intelligence Methodology, *Adv. Eng. Mater.*, 2007, **9**(1-2), p 105-113
11. A. Vaidya, Bancke, G., Sampath, S., Herman, H., Influence of Process Variables on the Plasma Sprayed Coatingsl an Integrated Study, *International Thermal Spray Conference*, May 28-30, 2001 (Singapore), 2001, p 1345-1349
12. A. Vaidya, T. Streibl, L. Li, S. Sampath, O. Kovarik, and R. Greenlaw, An Integrated Study of Thermal Spray Process-Structure-Property Correlations: A Case Study for Plasma Sprayed Molybdenum Coatings, *Mater. Sci. Eng. A Struct. Mater. Prop. Microstruct. Process.*, 2005, **403**(1-2), p 191-204
13. H. Zhang, H. B. Xiong, L. L. Zheng, A. Vaidya, L. Li and S. Sampath, Melting Behavior of In-Flight Particles and Its Effects on Splat Morphology in Plasma Spraying, *IMECE*, November 17-22, 2002 (New Orleans, LA), 2002, p 1-8
14. H.B. Xiong, L.L. Zheng, L. Li, and A. Vaidya, Melting and Oxidation Behavior of In-Flight Particles in Plasma Spray Process, *Int. J. Heat Mass Trans.*, 2005, **48**(25-26), p 5121-5133
15. M. Fukumoto, E. Nishioka, and T. Nishiyama, New Criterion for Splashing in Flattening of Thermal Sprayed Particles onto Flat Substrate Surface, *Surf. Coat. Technol.*, 2002, **161**(2-3), p 103-110
16. C. Escure, M. Vardelle, and P. Fauchais, Experimental and Theoretical Study of the Impact of Alumina Droplets on Cold and Hot Substrates, *Plasma Chem. Plasma Process.*, 2003, **23**(2), p 185-221
17. C.J. Li, H.L. Liao, P. Gougeon, G. Montavon, and C. Coddet, Experimental Determination of the Relationship between Flattening Degree and Reynolds Number for Spray Molten Droplets, *Surf. Coat. Technol.*, 2005, **191**(2-3), p 375-383
18. K. Shinoda, T. Koseki, and T. Yoshida, Influence of Impact Parameters of Zirconia Droplets on Splat Formation and Morphology in Plasma Spraying, *J. Appl. Phys.*, 2006, **100** (7), Art. no. 074903 (6 pages)
19. H.B. Xiong, L.L. Zheng, S. Sampath, R.L. Williamson, and J.R. Fincke, Three-Dimensional Simulation of Plasma Spray: Effects of Carrier Gas Flow and Particle Injection on Plasma Jet and Entrained Particle Behavior, *Int. J. Heat Mass Trans.*, 2004, **47**(24), p 5189-5200
20. S. Sampath, X. Jiang, A. Kulkarni, J. Matejicek, D.L. Gilmore, and R.A. Neiser, Development of Process Maps for Plasma Spray: Case Study for Molybdenum, *Mater. Sci. Eng. A Struct. Mater. Prop. Microstruct. Process*, 2003, **348**(1-2), p 54-66
21. S. Sampath, X.Y. Jiang, J. Matejicek, L. Prchlik, A. Kulkarni, and A. Vaidya, Role of Thermal Spray Processing Method on the Microstructure, Residual Stress and Properties of Coatings: An Integrated Study for Ni-5 wt.% Al Bond Coats, *Mater. Sci. Eng. A Struct. Mater. Prop. Microstruct. Process.*, 2004, **364**(1-2), p 216-231
22. M. Fukumoto, M. Shiiba, H. Kaji, and T. Yasui, Three-Dimensional Transition Map of Flattening Behavior in the Thermal Spray Process, *Pure Appl. Chem.*, 2005, **77**(2), p 429-442
23. L. Prchlik, J. Gutleber, and S. Sampath, Deposition and Properties of High-Velocity-Oxygen-Fuel and Plasma-Sprayed Mo-Mo2c Composite Coatings, *J. Therm. Spray Technol.*, 2001, **10**(4), p 643-655
24. Y.P. Wan, J.R. Fincke, X.Y. Jiang, S. Sampath, V. Prasad, and H. Herman, Modeling of Oxidation of Molybdenum Particles During Plasma Spray Deposition, *Metall. Mater. Trans. B Process Metall. Mater. Process. Sci.*, 2001, **32**(3), p 475-481
25. D.P. Guillen and B.G. Williams, In-Flight Oxidation of Aluminum in the Twin-Wire Electric Arc Process, *J. Therm. Spray Technol.*, 2006, **15**(1), p 63-71
26. M.P. Planche, H. Liao, and C. Coddet, Oxidation Control in Atmospheric Plasma Spraying Coating, *Surf. Coat. Technol.*, 2007, **202**(1), p 69-76
27. G. Espie, P. Fauchais, B. Hannoyer, J.C. Labbe, and A. Vardelle, Effect of Metal Particles Oxidation During the APS on the Wettability, *Heat and Mass Transfer under Plasma Conditions*, Annals of the New York Academy of Science, 1999, p 143-151
28. A. Vaidya, Thesis: Process Maps for Thermal Spray: A Fundamental Approach to Process-Property Relationships, Stony Brook University, 2004, p 30-32
29. V. Srinivasan, A. Vaidya, T. Streibl, M. Friis, and S. Sampath, On the Reproducibility of Air Plasma Spray Process and Control of Particle State, *J. Therm. Spray Technol.*, 2006, **15**(4), p 739-743
30. H.B. Xiong, L.L. Zheng, and T. Streibl, A Critical Assessment of Particle Temperature Distributions During Plasma Spraying: Numerical Studies for Ysz, *Plasma Chem. Plasma Process.*, 2006, **26**(1), p 53-72
31. M. Vardelle and P. Fauchais, Plasma Spray Processes: Diagnostics and Control?, *Pure Appl. Chem.*, 1999, **71**(10), p 1909-1918
32. V. Srinivasan, M. Friis, A. Vaidya, T. Streibl, and S. Sampath, Particle Injection in Direct Current Air Plasma Spray: Salient Observations and Optimization Strategies, *Plasma Chem. Plasma Process.*, 2007, **27**(5), p 609-623